THE ASTROPHYSICAL JOURNAL, 563:239–245, 2001 December 10

X-RAY OBSERVATIONS OF XTE J1550−564 DURING THE DECAY OF THE 2000 OUTBURST. II. TIMING

E. KALEMCI,[1] J. A. TOMSICK,[1] R. E. ROTHSCHILD,[1] K. POTTSCHMIDT,[2] AND P. KAARET[3]
Received 2001 May 3; accepted 2001 August 7

ABSTRACT

We investigate the timing behavior of XTE J1550−564 with the *Rossi X-Ray Timing Explorer* as the source made a transition to the hard state during the decay of the 2000 outburst. We detect a high-frequency quasi-periodic oscillation (QPO) at 65 Hz in one observation with a fractional rms amplitude of 4.9%. This is the first time that a high-frequency QPO has been detected in a transition to the hard state during outburst decay. We also observe low-frequency QPOs in the 0.36–4.1 Hz range and rich aperiodic variability. The changes in the temporal properties during the decay are very similar to the state transitions observed for other sources. We find a correlation between the low-frequency QPO and the break frequency in the continuum power spectra. We investigate the energy dependence of rms amplitudes of the QPOs. We compare these timing properties with those previously observed for XTE J1550−564 and other Galactic black hole candidates and discuss the implications for QPO models and black hole accretion.

Subject headings: black hole physics — stars: individual (XTE J1550−564) — X-rays: stars

1. INTRODUCTION

The soft X-ray transient XTE J1550−564 was first detected by the All-Sky Monitor (ASM; Levine et al. 1996) on board the *Rossi X-Ray Timing Explorer* (*RXTE*) in 1998 September (Smith 1998). The power spectra for XTE J1550−564 showed strong aperiodic variability as well as low-frequency (0.08–18 Hz; Cui et al. 1999; Remillard et al. 2001) and high-frequency (100–284 Hz; Remillard et al. 1999a; Homan et al. 2001) quasi-periodic oscillations (QPOs) during some of the *RXTE* observations. Previously detected high-frequency QPOs had low rms amplitudes ($\sim$1%) and occurred mostly when the source was bright. The low-frequency QPOs occurred for all of the spectral states. (The spectral states of the black hole binaries are not rigorously defined. See Homan et al. 2001 for a discussion of these states in XTE J1550−564.) The amplitudes of these low-frequency QPOs can be less than 1% in the soft state and as much as 17% in the hard state. Detailed discussion of classification of these QPOs and their properties can be found in Homan et al. (2001) and Remillard et al. (2001). The X-ray energy spectra usually show a soft component, which can be modeled as blackbody emission over a range of temperatures from a geometrically thin, optically thick disk, and a hard component modeled by a power law, which is thought to be the result of Compton upscattering of soft photons by an energetic electron corona (Sobczak et al. 1999). Both the X-ray spectra and the temporal properties are similar to the other Galactic black hole candidates (BHCs), and the recently measured mass function of $6.86 \pm 0.71\ M_{\odot}$ confirms its black hole nature (Orosz et al. 2001).

During the 1998 outburst, optical (Orosz, Bailyn, & Jain 1998) and radio (Campbell-Wilson et al. 1998) counterparts were identified. A superluminal ejection was discovered in the radio, establishing the source as a microquasar, similar to GRO J1655−40 and GRS 1915+105 (Hannikainen et al. 2001). It became active in X-rays again in 2000 April (Smith et al. 2000). The outburst reached its maximum ASM count rate at the end of 2000 April. The X-ray flux decayed over the next few months, and a transition to the hard state occurred. For more information about the X-ray spectrum and the radio properties of this outburst, see Tomsick, Corbel, & Kaaret (2001, hereafter Paper I), Corbel et al. (2001), and Miller et al. (2001a).

In this paper, we used the *RXTE*/Proportional Counter Array (PCA; see Bradt, Rothschild, & Swank 1993 for a description of *RXTE*) power spectra from observations of XTE J1550−564 made between May 16 and June 3, during the decay of the 2000 outburst. The detailed spectral analysis with *RXTE* and *Chandra* during the decay is covered by Paper I. We searched for high-frequency QPOs and studied the evolution of the low-frequency QPOs through the decay. We also investigated the evolution of the continuum parameters of the power spectra during the transition and compared the temporal properties to the previous observations and other BHCs.

2. OBSERVATIONS AND ANALYSIS

We used the standard *RXTE* data analysis software FTOOLS v5.0 to extract light curves. In the first two observations, the PCA data were accumulated in single-bit mode with 125 μs time resolution for two energy bands: 2–6 and 6–15 keV. Above 15 keV, we used the event mode with 8 μs time resolution and with 32 energy channels. After the second observation, the data were accumulated in the event mode with 125 μs time resolution and 64 energy channels. Typical integration times were 1–2 ks per observation. The XTE J1550−564 light curve and the exact integration times for our observations can be found in Paper I. We used all of the Proportional Counter Units (PCUs) that were on simultaneously. The observations were made after the loss of the propane layer for PCU 0, and we dealt with the additional background by assuming that PCU 0 and PCU 2 are identical and that the difference in the count rates between the two is the excess background from PCU 0. This excess background is added to the background obtained by using

[1] Center for Astrophysics and Space Sciences, Code 0424, University of California at San Diego, La Jolla, CA 92093-0424.
[2] Institut für Astronomie und Astrophysik, University of Tübingen, Waldhäuser Strasse 64, D-72076 Tübingen, Germany.
[3] Harvard-Smithsonian Center for Astrophysics, 60 Garden Street, Cambridge, MA 02138.

pcabackest. It should be noted that the background is used only to convert the power spectra to rms normalization (Berger & van der Klis 1994). For each observation, we computed the power spectra using IDL programs developed at the University of Tübingen for three energy bands, 2–6, 6–15, and 15–67 keV, as well as for the summed band of 2–67 keV. Above 67 keV, the source is not significantly above the background. The power spectra were corrected for the dead-time effects according to Zhang et al. (1995) with a dead time of 10 μs per event.

First, we searched for high-frequency QPOs by using short 1 s segments with a Nyquist frequency of 2048 Hz using the summed energy band. Except for observation 4 with its 65 Hz QPO, we did not detect any high-frequency QPOs. The 95% confidence upper limit on the rms amplitude is $\sim$3% before observation 6 and $\sim$5% after observation 6 for QPOs above 50 Hz. Then, using 128 s time segments, we investigated the low-frequency QPOs and the timing properties of the continuum up to 256 Hz.

3. RESULTS

We used observation 1 (Fig. 1*a*) as a test case to establish the model for fitting the power spectra. We started with a broken power law with the index of the power law below the break fixed to zero (hereafter we refer to this model as flat top or FT) to fit the continuum since this component is seen in all observations. To this we added a Lorentzian at $\sim$4 Hz to fit the low-frequency QPO. There were significant residuals at both the high- and low-frequency ends of the spectrum, and we obtained a poor fit with a χ^2 of 483 with 150 degrees of freedom. Adding a broad low-frequency bump (modeled by a Lorentzian) decreased the χ^2 to 235/147. The χ^2 dropped to 169/144 when another broad Lorentzian was added to fit the continuum at high frequencies. Even after this, we observed excess power at around twice the QPO frequency (first harmonic) and added a narrow Lorentzian, which reduced the χ^2 to 153/141. Figure 1*a* shows the power spectrum of observation 1 and the full model, which is FT plus 4 Lorentzians (high-frequency bump, low-frequency bump, QPO, and the harmonic). For the other observations, not all components are present at a significant level (see Table 1, Table 2, and the following discussion).

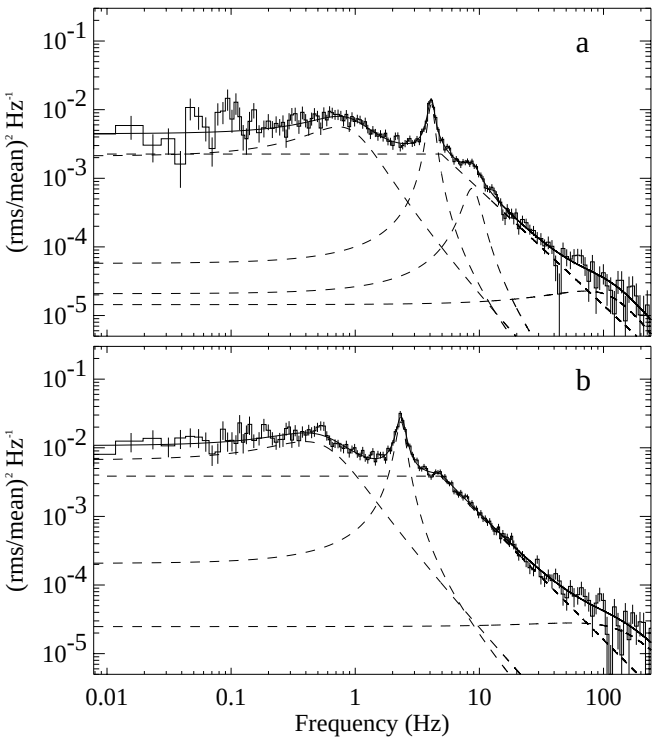

FIG. 1.—Power spectrum and best-fit model for observations 1(*a*) and 2(*b*). For observation 1, the model is FT (broken power law with the index of the power law below the break fixed to zero) plus two narrow Lorentzians for the QPO and its first harmonic plus two broad Lorentzians for the low-frequency and high-frequency noise components. For observation 2 (and also 3), the second harmonic is not statistically significant, and the model is FT plus QPO plus two broad Lorentzians. Dashed lines represent individual components; solid line is the overall fit to the data.

A low-frequency QPO occurs for each observation between observation 1 and observation 7, and the frequency of the QPO decreases from 4.09 to 0.36 Hz as the overall flux drops by a factor of 3 (see Table 1, Table 2, and Fig. 2). The amplitude stays around 10% and then decreases to 7.1% in observation 7 where it is last detected. The QPO is always below the break frequency. In observation 8, the 90% confidence upper limit for a QPO below the break frequency is 7.3%. The first harmonic is statistically significant in only the first observation and has an rms amplitude of 5.8%. For observations 2, 3, and 4, the 90% confidence upper limits of the rms amplitude of the harmonic is between 1.8% to 4.2% (see Table 2). The frequency of the first harmonic in observation 1 is slightly higher than twice the QPO frequency, and this may be due to the presence of a second harmonic, although adding another Lorentzian at the second harmonic frequency does not improve the fit. The QPO frequencies are correlated with the X-ray flux (Fig. 2) and the break frequencies (Fig. 3). The quality values (Q-values) are between 3 and 7. We also investigated the energy dependence of the rms amplitude of the low-frequency QPOs. Low count rates allowed us to use only three energy bands: 2–6, 6–15, and 15–67 keV, and Figure 4 shows the results. The rms amplitude shows a turnover in the first observation, an increase with energy in the second observation, and a decrease with energy in the remaining observations.

For the continuum parameters, the high-frequency bump is required for the first three observations (See Fig. 1 for observations 1 and 2). It peaks between 40 and 60 Hz, and its amplitude is between 7.1% and 11.8%. The observation 3 power spectrum is very similar to that of observation 2. For observation 4 there is no high-frequency bump, but a QPO is observed at 65 Hz. After observation 4, adding a high-frequency component does not improve the fit. The low-frequency noise, which peaks between 0.1 and 0.8 Hz, persists longer with an amplitude range of 7.6%–18.8%. It does not show a decreasing or increasing trend in time and disappears after observation 8 (see Table 1). Therefore, starting from observation 9, the power spectrum can be represented with just an FT component. The amplitude of the FT component increases from 16% in observation 1 to 43% in observation 12 (Fig. 2*b*). Both the power-law index and the break frequency show clear trends: the index (Fig. 2*c*) increases gradually while the break frequency (Fig. 2*d*) decreases. All these changes are consistent with a transition to a hard state (van der Klis 1995), and the energy spectrum also shows this transition (Paper I).

Perhaps the most important result is the detection of a high-frequency QPO in observation 4 at 65.0 $\pm$ 2.5 Hz (see

TABLE 1

POWER SPECTRA FIT PARAMETERS

MJD[a]	Observation	Flux[b]	FT rms (%)	FT Index	FT Break (Hz)	LF[c] Frequency (Hz)	LF rms (%)	HF[d] Frequency (Hz)	HF rms (%)	χ^2/ν
51,680.4.....	1	5.62	16.4 ± 0.1	−1.70 ± 0.05	5.04 ± 0.05	0.73 ± 0.03	10.1 ± 0.3	62.9 ± 30.5	8.7 ± 1.4	153.7/144
51,682.3.....	2	4.49	20.4 ± 1.2	−1.82 ± 0.08	4.87 ± 0.13	0.39 ± 0.03	12.8 ± 0.5	49.0 ± 145.9	11.8 ± 6.8	148.7/144
51,683.8.....	3	3.69	23.8 ± 1.3	−1.56 ± 0.04	2.41 ± 0.07	0.26 ± 0.01	9.1 ± 0.4	40.0 ± 26.6	7.1 ± 2.5	152.4/144
51,684.8.....	4[e]	3.20	23.9 ± 2.3	−1.48 ± 0.03	1.95 ± 0.12	0.10 ± 0.09	11.1 ± 2.4	...	...	110.7/139
51,686.3.....	5	2.68	24.8 ± 1.8	−1.39 ± 0.02	1.46 ± 0.07	0.23 ± 0.01	7.6 ± 0.6	...	...	145.5/147
51,687.2.....	6	2.38	27.1 ± 3.2	−1.32 ± 0.03	1.18 ± 0.09	0.16 ± 0.02	8.7 ± 1.2	...	...	123.1/130
51,688.8.....	7	1.85	27.0 ± 4.0	−1.33 ± 0.04	0.93 ± 0.07	0.17 ± 0.04	16.5 ± 4.2	...	...	130.5/130
51,690.8.....	8	1.43	28.7 ± 4.9	−1.25 ± 0.04	0.81 ± 0.07	0.14 ± 0.02	18.8 ± 1.7	...	...	192.0/133
51,692.6.....	9[f]	1.04	34.7 ± 3.9	−1.23 ± 0.03	0.22 ± 0.01	...	...	...	...	161.4/133
51,693.4.....	10	0.91	34.4 ± 2.1	−1.18 ± 0.02	0.16 ± 0.01	...	...	...	...	128.1/136
51,695.3.....	11	0.72	40.8 ± 8.3	−1.13 ± 0.03	0.14 ± 0.01	...	...	...	...	119.4/136
51,696.5.....	12	0.64	42.5 ± 7.3	−1.12 ± 0.02	0.09 ± 0.01	...	...	...	...	135.0/136
51,698.9.....	13	0.46	65.8 ± 48.8	−1.05 ± 0.05	0.05 ± 0.01	...	...	...	...	64.6/91

[a] Modified Julian Date (MJD = JD − 2,400,000.5) at the midpoint of the observation.
[b] Flux in 2.5–20 keV range, in units of 10^{-9} ergs cm^{-2} s^{-1}.
[c] Low-frequency noise component.
[d] High-frequency noise component.
[e] The high-frequency QPO at 65 Hz is detected in this observation.
[f] The 3.9 Hz QPO is detected in this observation.

Fig. 5). Within the restricted energy band of 2–28 keV, it has an F-test (Bevington & Robinson 1992) value of 0.99997. For the whole energy band (2–67 keV), it has an rms amplitude of 4.9% and a Q-value of 4.4. If we divide the light curve into three energy bands, the amplitude is 5.5% ± 1.3% for the 2–6 keV band and 4.7% ± 1.1% for the 6–15 keV band. The QPO is not detected in the third energy band (15–67 keV) with a 90% confidence upper limit amplitude of 4.5%. Thus, the strength of the high-frequency QPO is either constant or possibly decreasing in energy.

We also report the probable detection of another QPO in observation 9 at 3.9 ± 0.1 Hz with an F-test value of 0.9997 (see Fig. 6). This QPO is well above the break frequency of the FT component in contrast to the low-frequency QPOs that are observed in observations 1–7. This is indicative of a different origin for the 3.9 Hz QPO. In the 2–67 keV energy band, it has an rms amplitude of 5.8% ± 1.1% and a Q-value of ∼4. When we divide the light curve into two energy bands, we observe that the amplitude of the QPO increases substantially from 4.6% ± 1.7% in 2–8.5 keV to 8.3% ± 1.6% in 8.5–67 keV. Although we do not associate this QPO with the low-frequency QPOs, it may be related to the 65 Hz QPO, and we consider the implications of this possibility below. However, we note that there are reports of QPOs above the break frequency that are probably not related to the high-frequency QPOs (Remillard et al. 2001; Homan et al. 2001).

4. DISCUSSION

4.1. *The* 65 Hz *Quasi-Periodic Oscillation*

High-frequency QPOs have been observed in five Galactic BHCs. Two of them have fixed frequency over several observations: the 67 Hz QPO of GRS 1915+105 (Morgan, Remillard, & Greiner 1997) and the 300 Hz QPO of GRO J1655−40 (Remillard et al. 1999b).[4] The 184 Hz QPO of 4U 1630−47 has been observed only once (Remillard & Morgan 1999). XTE J1859+226 (Cui et al. 2000) has variable high-frequency QPOs (150–184 Hz). Finally, XTE J1550−564 also has variable high-frequency QPOs with a frequency range of 100–284 Hz (Remillard et al. 1999a;

[4] Recently, pairs of high-frequency QPOs were found in both sources (Strohmayer 2001a, 2001b).

TABLE 2

LOW-FREQUENCY QPO FIT PARAMETERS

Observation	QPO Frequency (Hz)	QPO rms (%)	FWHM (Hz)	Harmonic Frequency[a] (Hz)	Harmonic rms (%)
1	4.090 ± 0.015	10.4 ± 0.2	0.72 ± 0.04	8.75 ± 0.15	5.8 ± 0.4
2	2.337 ± 0.010	12.8 ± 0.3	0.44 ± 0.03	4.77 ± 0.04	<1.8[b]
3	1.119 ± 0.007	11.9 ± 0.3	0.26 ± 0.02	2.35 ± 0.02	<2.0[b]
4	0.962 ± 0.016	10.0 ± 0.8	0.28 ± 0.05	1.83 ± 0.05	<4.2[b]
5	0.678 ± 0.010	10.7 ± 0.6	0.19 ± 0.03	...	...
6	0.559 ± 0.012	11.4 ± 1.0	0.21 ± 0.05	...	...
7	0.355 ± 0.005	7.1 ± 0.9	0.05 ± 0.02	...	...
8	0.01–0.8[c]	<7.3[b]	0.15 × freq.[d]	...	...

[a] Frequency of the first harmonic.
[b] The 90% confidence upper limit.
[c] Frequency range searched (up to the break frequency).
[d] The width is fixed to 0.15 × QPO frequency (Q = 6.6).

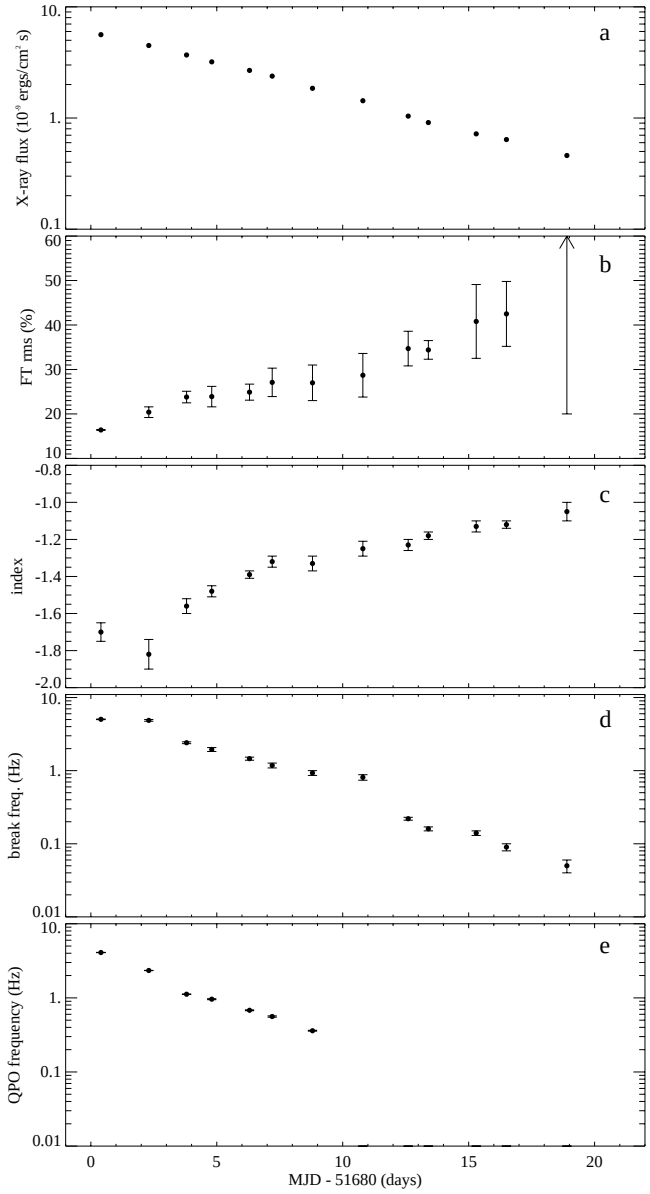

FIG. 2.—Change in the parameters of the power spectra as the flux decreases and the source makes a transition to the hard state. (*a*) The 2.5–20 keV X-ray flux; (*b*) the rms amplitude of the FT component; (*c*) the index of power law after the break in FT; (*d*) the break frequency; and (*e*) the QPO frequency.

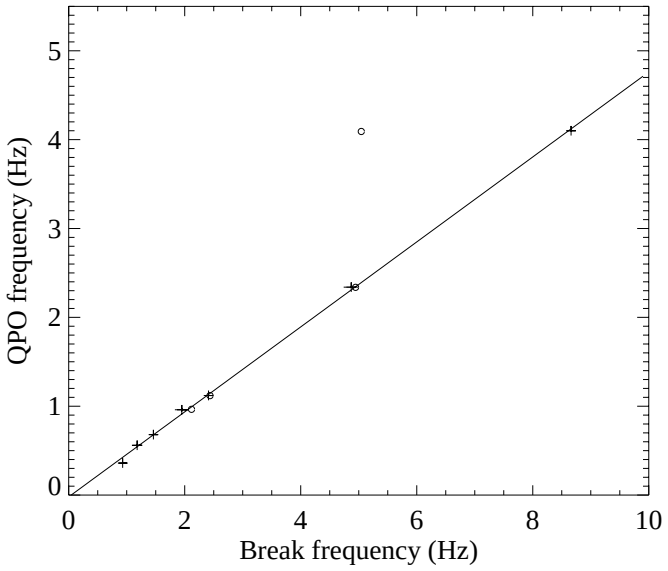

FIG. 3.—Correlation between the low-frequency QPO and the break frequency. Crosses indicate the case when we limit the model to FT plus two broad Lorentzians without the first harmonic; open circles indicate the case where we include a first harmonic even if it is not statistically significant. The correlation breaks down in observation 1 where a significant first harmonic is present. For the crosses, the fit is a straight line with $\nu_{\rm QPO} = (0.478 \pm 0.024)\nu_{\rm break} - (0.020 \pm 0.006)$ Hz, and the correlation coefficient is 0.9996.

Homan et al. 2001; Miller et al. 2001b). These high-frequency QPOs in XTE J1550−564 have rms amplitudes of around 1% for the energy band of 2–60 keV. Typically, the amplitudes increase with energy. The Q-values are between 4 and 13. They were observed in the very high state where the energy spectra show a strong power-law component (Remillard et al. 1999a).

The 65 Hz QPO we observe is not in the previously observed frequency range for XTE J1550−564, but it is close to the lower end of this frequency range as well as to the 67 Hz QPO observed for GRS 1915+105. The Q-value for the 65 Hz QPO is in the range usually seen for high-frequency QPOs, but the rms amplitude (4.9%) is higher than typical values seen for high-frequency QPOs. Another difference is that the amplitude for the 65 Hz QPO does not increase with energy as is usually observed for high-frequency QPOs. It is possible that the differences reflect the fact that the 65 Hz QPO was observed during the transition to the hard state, while other high-frequency QPOs have been detected when the systems were in the very high state. Although the properties of the 65 Hz QPO are not all typical of high-frequency QPOs, the properties fit well with trends that have been reported by other authors. For the high-frequency QPOs in XTE J1550−564, Homan et al. (2001) find a relationship between the QPO frequency and the location of the source on a color-color diagram. Using the same energy bands that were used in that work, we have calculated the values of the soft color and the hard color for observation 4. The soft color value of 0.91 and the hard color value of 0.08 are consistent with an extrapolation of the trend reported by Homan et al. (2001). High- and low-frequency QPOs are often seen simultaneously in the power spectra of BHCs as we observe for XTE J1550−564 during observation 4. Psaltis, Belloni, & van der Klis (1999) have reported on correlations between the frequencies of the high- and low-frequency QPOs and/or noise components in the power spectra of BHC and neutron star systems. The frequencies we measure for the observation 4 QPO pair are consistent with the Psaltis et al. (1999) correlation that includes the high-frequency QPOs for GRO J1655−40 and previous observations of XTE J1550−564. Overall, we believe that the evidence supports an association between the 65 Hz QPO and the previously observed QPOs.

For a 7 $M_\odot$ nonrotating black hole, the dynamical timescale at the last stable orbit is 314 Hz. High-frequency QPOs (65–284 Hz) therefore arise close to the black hole, where effects of general relativity are expected to be significant. Several models have been proposed to explain these QPOs. A complete list of these models can be found in a review by Remillard (2000). The three that can be applied to variable frequency QPOs are hot blobs in the inner edge of

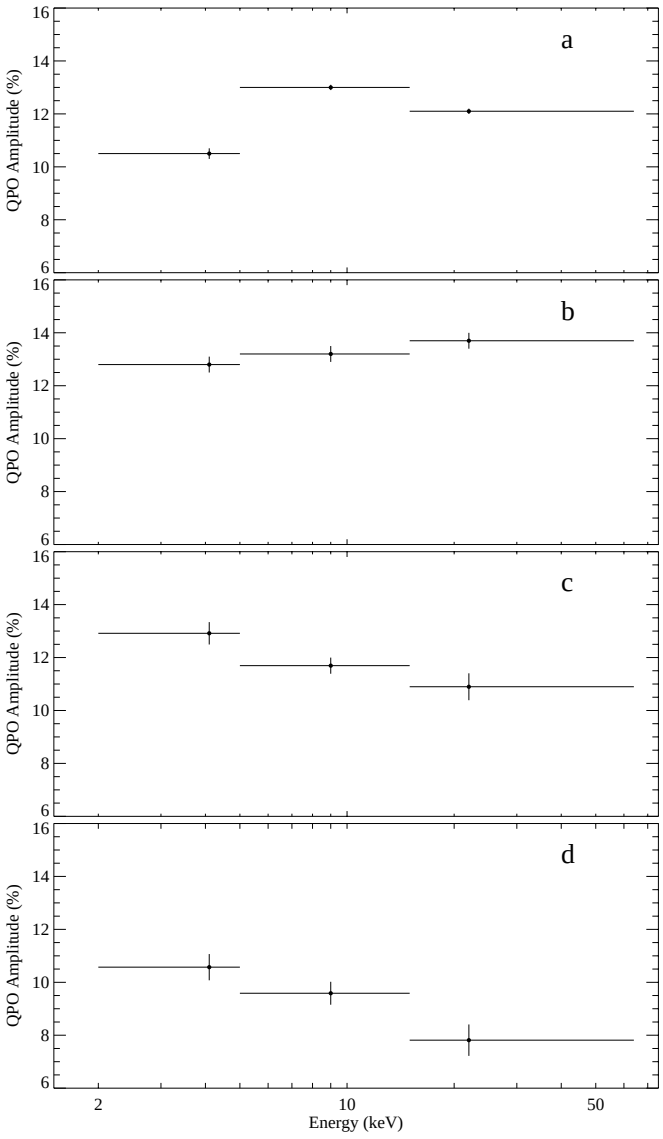

FIG. 4.—Low-frequency QPO amplitude as a function of energy. (*a*) Observation 1; (*b*) observation 2; (*c*) observation 3; and (*d*) combination of observations 4 through 7.

the disk (with Keplerian QPO frequency), Lense-Thirring precession of the tilted circular orbits of a spinning black hole (LT model; Cui, Chen & Zhang 1998; Cui, Zhang & Chen 1998), and diskoseismic mode oscillations (Nowak & Wagoner 1993; Nowak & Lehr 1998). To produce variable frequency QPOs, the first two require a change in the inner radius of the disk (Cui et al. 2000) and the last can have variable frequency if the disk thickness h changes as a function of radius r (Nowak & Lehr 1998). If the 65 Hz QPO in XTE J1550−564 is related to the 284 Hz QPO observed previously, then any model must explain a factor of 4 change in frequency. It was argued by Nowak & Wagoner (1993) that the change in frequency due to changes in h/r is small, and g-mode oscillations are expected to produce low-amplitude ($\sim$1%) QPOs. The LT mechanism, on the other hand, can account for the change in frequency. It requires high-frequency QPOs to occur during state transitions because the accretion disk is expected to be realigned with the equatorial plane for stable accretion due to the Bardeen-Petterson effect, and the QPO should disappear in time

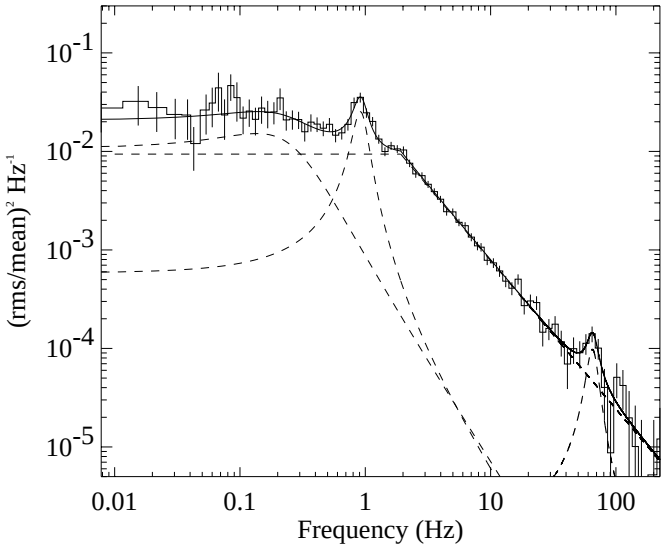

FIG. 5.—Power spectrum for observation 4 with QPOs at 0.96 and 65 Hz. The high-frequency QPO has 4.9% rms amplitude and a quality factor of 4.4.

(Cui et al. 1998). This is consistent with the occurrence of the 65 Hz QPO during a transition. However, it is not clear how the luminosity variations can be produced by LT precession (Nowak & Lehr 1998; Cui et al. 1998). Although hot blobs at the inner edge (or in a region where disk emissivity peaks; Cui et al. 1998) can explain the high-frequency QPOs and the change in the frequency, there are reports that this model is incompatible with the spectral results (Cui et al. 1998).

All the models described above have the high-frequency QPO originating in the accretion disk. Remillard et al. (1999a) observe that the high-frequency QPOs emerge in XTE J1550−564 when the disk temperature ($T_{\rm col}$) is high ($>$0.84 keV). In contrast, the disk-blackbody component is not detected in the *RXTE* band for observation 4, indicating a disk temperature less than about 0.4 keV (Paper I). This means that the power-law component provides nearly

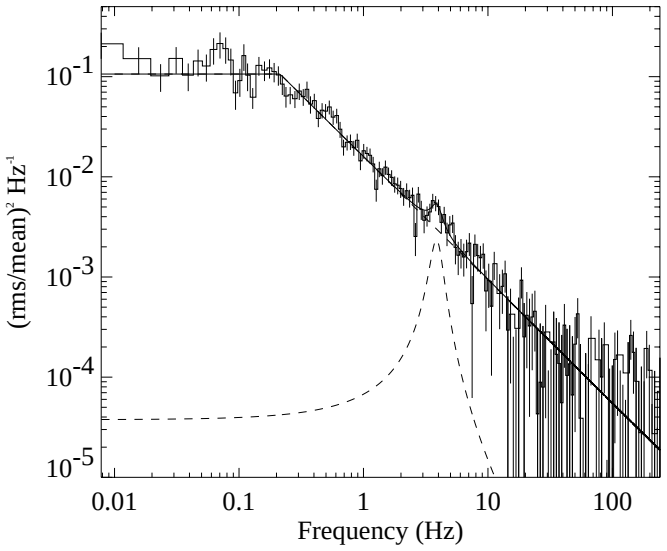

FIG. 6.—Power spectrum for observation 9 with a probable detection of a QPO at 3.9 Hz. This QPO has 5.8% rms amplitude and a quality value of $\sim$4.

all of the 2–150 keV luminosity. The properties of previously observed QPOs seem to correlate much better with those of hard X-rays (perhaps of a Comptonizing corona; Cui 1998). Our observations seem to support this trend since we observe a strong high-frequency QPO without a disk component in the spectrum. Note that this is not proof that the origin of high-frequency QPOs cannot be in the disk since the oscillations in the disk flux (soft X-rays and UV) can modulate the input to the corona.

As discussed above, the high QPO frequencies may be associated with the Keplerian or the LT timescale for the inner edge of the accretion disk. Under this assumption, one can use the QPO frequencies to trace the radius of the inner edge of the accretion disk. The highest frequency observed in XTE J1550−564 is 284 Hz, which likely originates close to the black hole. We designate $R_{\rm min}$ to be the inner radius when the 284 Hz high-frequency QPO is observed. This radius may be close to the marginally stable orbit. If we assume that the 65 Hz QPO in observation 4 and the 3.9 Hz QPO in observation 9 are related to the 284 Hz QPO, then for Keplerian timescales the inner edge moves to $2.7R_{\rm min}$ for observation 4 and to $17R_{\rm min}$ for observation 9. The change in radius for a LT timescale is smaller: $1.6R_{\rm min}$ and $4.2R_{\rm min}$, respectively.

One of the models devised to understand the energy spectra of accreting BHCs is the advection-dominated accretion flow (ADAF) model (Narayan, McClintock, & Yi 1996). Esin, McClintock, & Narayan (1997) developed a model consisting of an ADAF and an optically thick outer accretion disk and used this model to explain the spectral changes seen in the BHC Nova Muscae. In the context of this model, the different spectral states can be explained by changes in the mass accretion rate and the inner edge of the optically thick accretion disk. This model predicts that the inner edge of the accretion disk moves away from the black hole during a transition to the hard state, which is consistent with the increasing of the inner radius discussed previously. If the association of the high-frequency QPOs to the Keplerian timescales at the inner edge of the disk is correct, then the inner edge of the disk moves substantially even in the intermediate/very high state where the QPOs have been observed in the 100–284 Hz range.

4.2. *Low-Frequency QPOs and Continuum Parameters during State Transition*

Observations by Cui et al. (1999) in the beginning of the 1998 outburst and the observations reported here demonstrate the behavior of the temporal properties of XTE J1550−564 during the state transitions between the hard and the very high states. As the flux decreases and the source makes its transition to the hard state, the QPO frequency decreases along with the break frequency while the amplitude of the FT component and the index of the FT power-law component increase. The reverse was seen by Cui et al. (1999) when the source made its transition to the very high state. The temporal properties for XTE J1550−564 during the transition to the hard state are very similar to what has been observed for the BHC 4U 1630−47 (Tomsick & Kaaret 2000). For 4U 1630−47, a QPO was present that dropped in frequency from 3.4 to 0.2 Hz as the source flux decayed. Also, the evolution of the continuum parameters were similar, with an increase in the amplitude of the FT component and a drop in the break frequency. However, for 4U 1630−47, a sharp transition was seen with most of the changes in the temporal properties occurring in less than 2 days. For XTE J1550−564, the QPO was present and the FT rms amplitude was relatively high in our first observation. It is possible that a sharp transition might have happened before our observations began. One interesting feature generally overlooked in describing the state transitions is the change in the index of the power-law component in the power spectrum. This regular change of index during state transitions is observed in XTE J1550−564 and also in GRO J1655−40 (Mendez, Belloni, & van der Klis 1998) and may have implications for the models of aperiodic variability such as shot-noise models (Pottschmidt et al. 1998 and references therein).

The XTE J1550−564 power spectra show a correlation between the break frequency and the central frequency of the low-frequency QPO. The fact that the break frequency follows the QPO frequency was reported by Cui et al. (1999) for XTE J1550−564, and this trend is observed in other black holes and neutron star systems (Wijnands & van der Klis 1999). Figure 3 shows this correlation for two cases; crosses indicate the cases where we do not include the first harmonic in the fit, and open circles indicate the cases where we include a first harmonic (even if it is not statistically significant). Except for in observation 1, including the harmonic does not alter the break frequencies significantly. For observation 1, the fit without the harmonic yields a break frequency of 8.6 Hz, compared to 5.0 Hz with the harmonic. Some scatter is present in the correlations reported by Wijnands & van der Klis (1999), and they attribute this to the complex structure of the QPO and its harmonics. Similarly, our correlation breaks down in observation 1 when we include the first harmonic in the fit (Fig. 3, *open circles*). If we do not include the first harmonic, there is no scatter and the correlation is superb with a correlation coefficient of 0.9996. But the fact that the correlation breaks down for the full model and also that the break frequencies are almost twice the QPO frequencies leads us to believe that the first harmonic drives the break frequency to the centroid frequency of the first harmonic.

Previous results by Cui et al. (1999), Homan et al. (2001), and Remillard et al. (1999a) show that the amplitude of both the low- and high-frequency QPOs increase with energy in XTE J1550−564. For some cases there is a turnover in this relation, but it is at high energies (>60 keV) as shown by Kalemci, Tomsick, & Rothschild (2000). This kind of turnover is observed also in GRS 1915+105 (Tomsick & Kaaret 2001). In contrast, we observed a turnover in observation 1 at 10 keV and a decreasing relation after observation 3 (see Fig. 4). A decrease in the amplitude as energy increases was also seen in the hard state of Cyg X-1 (Rutledge et al. 1999), and for some low-frequency QPOs (0.06–0.2 Hz) in GRS 1915+105 (Morgan et al. 1997). A detailed investigation of the amplitude versus energy relation in XTE J1550−564 is the subject of future work.

5. SUMMARY AND CONCLUSIONS

The most important result of this paper is the detection of a high-frequency QPO at 65 Hz since it is the first time a high-frequency QPO has been observed in a transition to the hard state during the outburst decay. It has relatively high amplitude of 4.9% and a Q-value of 4.4. During the time the QPO was observed, the *RXTE* energy spectrum was dominated by a power-law component and the disk

component was not detected (Paper I). Although the evidence supports its association with the previously observed high-frequency QPOs, it is stronger in amplitude and does not show an increasing amplitude with increasing energy. We considered three mechanisms to explain the variable high-frequency QPOs: self-illuminating clumps in the inner accretion disk, Lense-Thirring precession, and diskoseismic g-mode oscillations. The diskoseismic oscillation model is unlikely to explain such a high amplitude. We also report the probable detection of a QPO at 3.9 Hz during an observation that occurred after the one where 65 Hz QPO was detected. This QPO is well above the break frequency, and it is unlikely that it is related to the other low-frequency QPOs. It is possible that the 3.9 Hz and 65 Hz QPOs are related and that they provide information about the location of the inner radius of the accretion disk.

Another result is the correlation between the low-frequency QPOs and the break frequencies and the fact that it breaks down when a complex QPO structure is present. We also show that the change in temporal properties in the transition to the hard state is the mirror image of the change in the temporal properties in hard to very high state transition (Cui et al. 1999). The main features of the transition are a drop in the low-frequency QPO frequency from 4.1 to 0.36 Hz, a decrease in the break frequency from 5 to 0.6 Hz, an increase in FT amplitude from 14% to 42%, and an increase of the power-law index of the power spectra from -1.8 to -1.1 (see Table 1). From these data, it is not clear whether a sharp transition exists in temporal properties as reported for 4U 1630−47 (Tomsick & Kaaret 2000). We should be able to conclude whether a sharp transition exists by combining our data with the data taken prior to our observations.

E. K. acknowledges useful discussions with Jörn Wilms and Wayne Coburn. The authors would like to thank all scientists who contributed to the Tübingen Timing Tools. This material is based in part upon work supported by the National Aeronautics and Space Administration under grants NAG 5-30120 and NAG 5-10886. E. K. was partially supported by TÜBITAK. K. P. is supported by DFG grant Sta 173/25-3 and a travel grant from the DAAD and would like to thank CASS for its hospitality. P. K. acknowledges partial support from NASA grant NAG 5-7405.

REFERENCES

Berger, M., & van der Klis, M. 1994, A&A, 292, 175
Bevington, P. R., & Robinson, D. K. 1992, Data Reduction and Error Analysis for the Physical Sciences (2d ed.; New York: McGraw-Hill)
Bradt, H. V., Rothschild, R. E., & Swank, J. H. 1993, A&AS, 97, 355
Campbell-Wilson, D., McIntyre, V., Hunstead, R., Green, A., Wilson, R. B., & Wilson, C. A. 1998, IAU Circ. 7010
Corbel, S., et al. 2001, ApJ, 554, 43
Cui, W. 1998, in ASP Conf. Ser. 161, High Energy Processes in Accreting Black Holes, ed. J. Poutanen & R. Svensson (San Francisco: ASP)
Cui, W., Chen, W., & Zhang, S. N. 1998, in Proc. Third William Fairbank Meeting on the Lense-Thirring effects, ed. L.-Z. Fang & R. Ruffini (Rome: Univ. La Sapienza)
Cui, W., Shrader, C. R., Haswell, C. A., & Hynes, R. I. 2000, ApJ, 535, L123
Cui, W., Zhang, S. N., & Chen, W. 1998, ApJ, 492, 53
Cui, W., Zhang, S. N., Chen, W., & Morgan, E. H. 1999, ApJ, 512, L43
Esin, A. A., McClintock, J. E., & Narayan, R. 1997, ApJ, 489, 865
Hannikainen, D., et al. 2001, Ap&SS, 276, 45
Homan, J., et al. 2001, ApJS, 132, 377
Kalemci, E., Tomsick, J. A., & Rothschild, R. E. 2000, AAS/High Energy Astrophysics Division, 32, 3105
Levine, A. M., et al. 1996, ApJ, 469, L33
Mendez, M., Belloni, T., & van der Klis, M. 1998, ApJ, 499, L187
Miller, J. M., et al. 2001a, preprint (astro-ph/0103215)
———. 2001b, ApJ, in press
Morgan, E. H., Remillard, R. A., & Greiner, J. 1997, ApJ, 482, 993
Narayan, R., McClintock, J. E., & Yi, I. 1996, ApJ, 457, 821
Nowak, M., & Lehr, D. 1998, in Theory of Black Hole Accretion Disks, ed. M. A. Abromowicz, B. Bjvrnsson, & J. E. Pringle (Cambridge: Cambridge Univ. Press), 233
Nowak, M. A., & Wagoner, R. V. 1993, ApJ, 418, 187
Orosz, J., Bailyn, C., & Jain, R. 1998, IAU Circ. 7009
Orosz, J. A., van der Klis, M., McClintock, J. E., Jain, R. K., Bailyn, C. D., & Remillard, R. A. 2001, Astron. Telegram, 70
Pottschmidt, K., Koenig, M., Wilms, J., & Staubert, R. 1998, A&A, 334, 201
Psaltis, D., Belloni, T., & van der Klis, M. 1999, ApJ, 520, 262
Remillard, R. A. 2000, in ASP Conf. Ser. 229, Evolution of Binary and Multiple Star Systems, ed. P. Podsiaklowski, S. Rappaport, A. King, F. D'Antona, & L. Burderi (San Francisco: ASP), 503
Remillard, R. A., McClintock, J. E., Sobczak, G. J., Bailyn, C. D., Orosz, J. A., Morgan, E. H., & Levine, A. M., 1999a, ApJ, 517, L127
Remillard, R. A., & Morgan, E. H. 1999, AAS Meeting, 195, 3702
Remillard, R. A., Morgan, E. H., McClintock, J. E., Bailyn, C. D., & Orosz, J. A., 1999b, ApJ, 522, 397
Remillard, R. A., Sobczak, G. J., Muno, M. P., & McClintock, J. E. 2001, ApJ, submitted
Rutledge, R. E., et al. 1999, ApJS, 124, 265
Smith, D. A. 1998, IAU Circ. 7008
Smith, D. A., et al. 2000, IAU Circ. 7399
Sobczak, G. J., McClintock, J. E., Remillard, R. A., Levine, A. M., Morgan, E. H., Bailyn, C. D., & Orosz, J. A. 1999, ApJ, 517, L121
Strohmayer, T. E. 2001a, ApJ, 552, L49
———. 2001b, ApJ, 554, L169
Tomsick, J. A., Corbel, S., & Kaaret, P. 2001, ApJ, 563, 229 (Paper I)
Tomsick, J. A., & Kaaret, P. 2000, ApJ, 537, 448
———. 2001, ApJ, 548, 401
van der Klis, M. 1995, in X-Ray Binaries, ed. W. H. G. Lewin, J. van Paradjs, & E. P. J. van den Heuvel (Cambridge: Cambridge Univ. Press), 252
Wijnands, R., & van der Klis, M. 1999, ApJ, 514, 939
Zhang, W., Jahoda, K., Swank, J. H., Morgan, E. H., & Giles, A. B. 1995, ApJ, 449, 930